ISSN 2411-3336; e-ISSN 2541-9404

JOURNAL OF MINING INSTITUTE

Zapiski Gornogo instituta

Journal homepage: pmi.spmi.ru

Research article

Geology

Lithological-geochemical specifics and genesis of terrigenous-carbonate rocks of the Lower Evenki Member (Middle Cambrian, West of the Siberian Platform)

Sofya I. Merenkova[1,2]✉, **Evgeniya V. Karpova**[3], **Aleksei Yu. Puzik**[4], **Vladimir A. Litvinskii**[5], **Yuliya V. Shuvalova**[5], **Margarita A. Volkova**[4], **Aleksei A. Medvedkov**[3,6]

[1] *Shirshov Institute of Oceanology of RAS, Moscow, Russia*

[2] *Schmidt Institute of Physics of the Earth RAS, Moscow, Russia*

[3] *Lomonosov Moscow State University, Moscow, Russia*

[4] *Perm State National Research University, Perm, Russia*

[5] *Borissiak Paleontological Institute of RAS, Moscow, Russia*

[6] *Institute of Geography RAS, Moscow, Russia*

***How to cite this article*:** Merenkova S.I., Karpova E.V., Puzik A.Yu., Litvinskii V.A., Shuvalova Yu.V., Volkova M.A., Medvedkov A.A. Lithological-geochemical specifics and genesis of terrigenous-carbonate rocks of the Lower Evenki Member (Middle Cambrian, West of the Siberian Platform). Journal of Mining Institute. 2025. Vol. 276. Iss. 2, p. 71-88.

Abstract

The lithological features of the Middle Cambrian sublittoral-littoral deposits of the Lower Evenki Member (Baykit Anteclise) have been refined. Four types of dolomites are identified: with stromatolitic texture, clotted-peloidal, replacement crystalline without preservation of the protolith primary structures, and replacement variably-crystalline with relict silt-pelitic structure. Post-sedimentary alterations of the rocks are associated with multi-stage dolomitization processes – early, syngenetic (in dolomite with stromatolitic texture and/or bacterial structures) and later (in replacement dolomites and silt-sandstones with dolomitic cement). The isotopic composition of carbon and oxygen in carbonates is analyzed. The elemental composition of carbonate, terrigenous-carbonate, carbonate-terrigenous, and terrigenous rocks is studied. A heat map with clustering was used to visualize the general pattern of enrichment by various elements. Carbonate lithology types are significantly enriched in Co, Cr, Sc, Rb and depleted in Cu, Zn, Li, Ba, Pb, and Sr in comparison with carbonate Clarke values. The nature of the positive Eu anomaly is investigated; its origin is attributed to Eu-bearing minerals in the terrigenous component of the rocks, rather than to hydrothermal solutions. No direct correlation is observed between the Rare Earth Element (REE) content and the amount of terrigenous admixture, thus the influence of reducing conditions or the composition of the dolomitizing fluid on the REE distribution cannot be ruled out. Terrigenous varieties are depleted in Cu, Zn, Pb, Ba, Th, U relative to the Clarke values for clays and clay shales. When normalized to PAAS, dolomitic argillites, dolomitic siltstones, sandstones, and silt-sandstones generally show enrichment in HREE relative to LREE. The source of the terrigenous clastic material was the Precambrian terranes of the Yenisei Ridge, formed by island-arc complexes, and recycled sedimentary material.

Keywords

Siberian Platform; Middle Cambrian; Evenki Formation; rare and rare earth element geochemistry; carbon and oxygen isotopic composition; depositional environments

Funding

The study was carried out within the framework of the State assignment of the Institute of Oceanology RAS (topic FMWE-2024-0020). Isotopic studies were supported by the State assignment of the Paleontological Institute RAS. Partial performance of the work was carried out within the framework of the State assignments of the Institute of Physics of the Earth RAS and the Institute of Geography RAS.

Received: 03.10.2024 ***Accepted: 10.04.2025*** ***Online: 14.10.2025*** ***Published: 29.12.2025***

Journal of Mining Institute. 2025. Vol. 276. Iss. 2. P. 71-88

Introduction

Determining the formation conditions of lagoon, sabkha, tidal flat, and other transitional zone deposits between land and marine basins is one of the most challenging problems in the study Paleozoic and earlier deposits. Despite active research on terrigenous-carbonate and carbonate-evaporite sequences formed in coastal-shallow marine and subaerial settings of the interior of the Siberian Platform, Cambrian sections remain insufficiently studied due to difficulties in dating the deposits and the significant uniqueness of the facies, which lack modern analogues.

In the Baykit zone, the Evenki Formation is subdivided into two members [1], or alternatively, the Chernostrovskaya and Velminskaya formations are distinguished within the Evenki Series (Fig.1, *a*), which conformably overlie the rocks of the Olenchiminskaya Formation. The lower member (220-325 m) at the base consists of uniform red and less frequently green silty dolomitic marls, often saline and sulfate-bearing, with gray clayey dolomites and limestones. Its upper part has a more terrigenous composition, dominated by dolomitic argillites, siltstones, marls, and sandstones [1]. In contrast to the lower member, the upper one (190-205 m) is more carbonate-rich and includes red-colored dolomites, dolomitic marls, and siltstones, with cherry-brown and greenish marls and interbeds of argillites. The lower member is attributed to the Mayan Stage of the Middle Cambrian, the upper – to the Upper Cambrian [1, 2].

The outcrop of the Lower Evenki Member is located on the right bank of the Podkamennaya Tunguska River near the settlement of Sulomai (Evenki Municipal District, Krasnoyarsk Region) (Fig.1, *b*, *c*)[1]. A detailed description of the section with a total thickness of 61.4 m is presented in [3]. According to the facies-paleogeographical scheme of the Siberian Platform for the Mayan Age of the Cambrian [2], the area of development of the Evenki Formation rocks lies within the field of supratidal plains (sabkhas). A hypothesis exists regarding the formation of the Evenki Formation with a leading role of storm sedimentation processes [4]. Previously, it was shown in [3, 5] that in terms of lithological composition, the rocks of the Lower Evenki Member of the Podkamennaya Tunguska

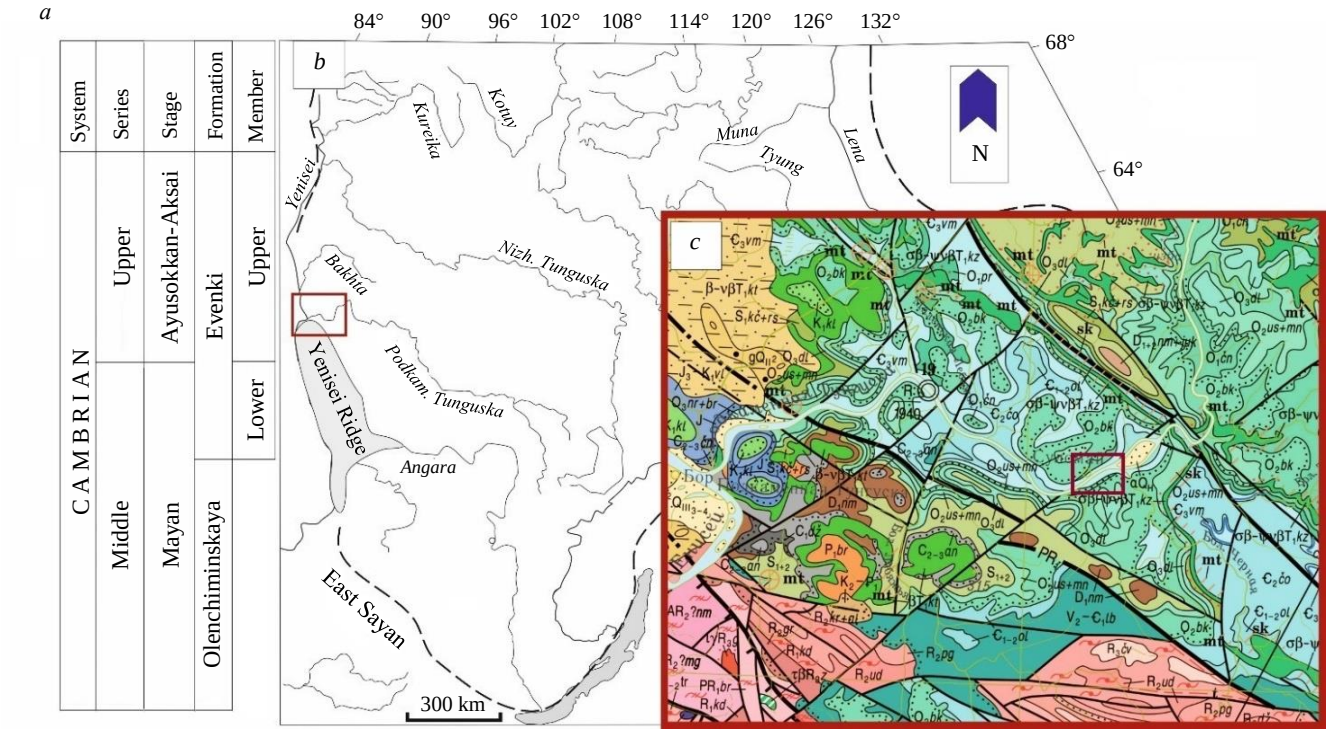

Fig.1. Position of the studied section of the Evenki Formation: *a* – stratigraphic column; *b*, *c* – regional map

[1] State Geological Map of the Russian Federation. Scale 1:1,000,000 (third generation). Angaro-Yenisei Series. Sheet P-46 – North Yenisei. Explanatory Note. St. Petersburg: Cartographic Factory of VSEGEI, 2010, p. 470.

River are most similar to littoral formations within the carbonate-evaporite formation of the Vendian – Lower Cambrian of the Nepa-Botuoba Anteclise [6, 7]. Based on this, an assumption was put forward [3, 5] that the studied facies of the Evenki Formation belong predominantly to upper littoral settings with possible episodic conditions of the lower supralittoral during a relative sea-level fall. Characteristic sabkha features such as lenses, crusts, nodules of gypsum and anhydrite are not observed in the studied section of the Evenki Formation, only rare relict dissolution pores in silty-clayey dolomites are present. Wave ripples, textures of con-sedimentary deformations, thin low-angle wavy, low-angle oblique, and graded bedding are present. The rocks contain dolomite lithoclasts. Based on the described features of the Lower Evenki Member section in the lower reaches of the Podkamennaya Tunguska River and an analysis of the genesis of modern and ancient sabkha and some coastal facies, it was concluded that the studied rocks formed predominantly in tidal flat settings, associated with coastal sabkhas [5].

Within the Nepa-Botuoba Anteclise, Vendian terrigenous rocks formed in coastal-marine settings of tidal coast with sabkhas are studied in much greater detail [8, 9], as Vendian – Cambrian deposits of this area are associated with oil and gas fields. Similarly, due to the gas potential of the deposits, researchers are interested in the formation conditions, diagenetic and post-diagenetic alterations of Middle Ordovician sabkha dolomites in the Ordos Basin (China) [10-12].

This work aims to study the geochemical features and conduct additional petrographic investigations of rocks formed in tidal flat settings during the Middle Cambrian. The results provide insights into the nature of post-sedimentary alterations, geochemical characteristics, and processes of dolomitization of carbonate and terrigenous-carbonate rocks, and when considering carbonate-terrigenous and terrigenous deposits – into the influence of source provinces.

Methods

Thin section description and photography were performed using a Zeiss Axio Scope microscope and Zeiss ZEN core software.

For the analysis of the carbon and oxygen isotopic composition, bulk crushed powder samples of dolomites were used. Stable isotope ratio analysis itself took place at the Instrumental Analytics Facility of the Borissiak Paleontological Institute of the RAS (PIN RAS). The obtained analytical material was transferred into tightly sealed microcentrifuge tubes. Using a microbalance, aliquots of each crushed analytical material were weighed into borosilicate glass vials. The mass of a single aliquot ranged from 330 to 390 μg. A volume of 0.05 ml of concentrated orthophosphoric acid solution was added to each vial with the carbonate sample aliquot using an automated dispensing system. The reaction between the carbonate aliquot and the acid lasted for 1 h in a thermostatted rack at a temperature of 70.1±0.1 °C. Analysis of the stable carbon and oxygen isotope ratios was performed using an Isoprime precisION-IsoFLOW instrument complex (Elementar UK Ltd., UK). The international standard IAEA NBS18 and an in-house laboratory standard KH2 were used for quality control. The reproducibility of the results was assessed by the standard deviation, which for $\delta^{13}C$ and $\delta^{18}O$ was 0.1 ‰ PDB.

Laboratory analytical studies of the elemental composition of carbonate, terrigenous-carbonate, carbonate-terrigenous, and terrigenous rocks were performed at the Center for Collective Use of Perm State National Research University. A 0.1 g aliquot of a ground sample was subjected to acid decomposition. The aliquot was placed in glassy carbon crucibles, moistened with laboratory-grade water, followed by the addition of 0.5 cm^3 of perchloric acid (70 %), 3 cm^3 of hydrofluoric acid (40 %), and 0.5 cm^3 of nitric acid (65 %). The crucibles were covered with lids and heated for 30 min at a temperature of 130 °C on an RP-1 hotplate (NPP Tomanalit LLC, Russia). Then, the lids were removed, and the solution was evaporated at 170-180 °C. Subsequently, the crucibles were cooled, the walls were rinsed, and evaporated again until moist salts remained. Then, 2 cm^3 of hydrochloric acid and 0.2 cm^3 of a 0.1M boric acid solution were added, and the solutions were evaporated to a volume of

0.7 cm^3. The resulting solutions were transferred to polyethylene tubes, and an indium internal standard was added. The content of trace elements was determined using a Bruker AURORA M90 inductively coupled plasma mass spectrometer (ICP-MS) (USA).

As statistical tools for interpreting the trace element data, a heat map with complete-linkage clustering and Pearson correlation coefficients were used. The heat map is based on a method for detecting outliers in a data array [13].

Results

Characteristics of lithological types of deposits. Based on the study of the most representative samples of carbonate, terrigenous-carbonate, and carbonate-terrigenous rocks in thin sections, the following types can be distinguished (Table 1):

• Stromatolitic dolomites.

• Clotted-peloidal dolomites.

• Replacement variably-crystalline dolomites without preservation of the protolith's primary structures.

• Replacement variably-crystalline dolomites, with a relict silt-pelitic structure of the protolith, spotty ferruginized; or with an admixture (up to 35-40 %) of residual silt-sandy material.

• Sandstones of various structural types and arkosic silt-sandstones with basal dolomitic cement.

The content of feldspars (Fsp) is given based on the calculation of the normative mineral composition using the O.M.Rosen method [14, 15].

Table 1

Lithological types of rocks of the Evenki Formation

Lithotype	Sample	Description
Stromatolitic dolomites	SL-3/1 SL-1/1 SL-1/6	Microcrystalline dolomite (0.01-0.05 mm), locally fine-grained (up to 0.1 mm), with stromatolitic texture. Consists of micritic laminae alternating with sparitic laminae of fine-crystalline dolomite. Contains finely dispersed admixture (0.5-1 %) of silt-sized, rarely very fine-sand-sized quartz, Fsp, and mica. Total Fsp content ranges from 2.4 to 6.2 %
	SL-6/43	Bacterial dolomite, locally with stromatolitic texture. Consists of continuous micritic laminae and films alternating with micro-laminae and micro-lenses of clotted material. Contains areas of sparitic texture, locally acquiring a fenestral appearance with voids filled by fine- to medium-crystalline calcite. Cyanobacterial formations have a spherical shape (*Renalcis*?), micro-oncolites, katagraphs, and clots are identified. Contains finely dispersed admixture (0.5-1 %) of silt-sized, rarely very fine-sand-sized quartz, Fsp, and mica. Total Fsp content is 7.5 %
Clotted-peloidal dolomites	SL-6/8	Clotted-peloidal dolomite, consisting of aggregates of micritic texture of rounded shape. In separate areas, remnants of cyanobacteria are found. The rock is non-laminated, contains areas of continuous micritic and clear-crystalline dolomite as a cementing mass. Contains an admixture of clastic material (3-5 %) in the form of poorly rounded grains of quartz, mica, Fsp of silt to very fine-sand size. Single grains of zircon and micro-nodules of glauconite and collophane (up to 0.07 mm) are observed. The rock is weakly porous, with voids filled by authigenic clear-crystalline dolomite and quartz. Total Fsp content is 3.4 %
	SL-6/9 SL-6/18	Represented by several layers differing in structure and composition – clotted-peloidal dolomite, clear-crystalline replacement dolomite with an admixture of gradationally distributed (up to 25 %) very fine-sandy material represented by quartz, Fsp, and mica. Total Fsp content is 10.9-12.9 %
Replacement crystalline dolomites without preservation of primary protolith structures	SL-2/2	Replacement variably-crystalline dolomite (crystal size from 0.03-0.05 to 0.12 mm), homogeneous, without preservation of signs of primary structure and texture, with residual grains of quartz, muscovite, plagioclase of silt and very fine-sand size (total impurity content not more than 1-2 %), evenly distributed; with dissolution pores filled by fine- to very fine-crystalline calcite (1-2 %). Total Fsp content is 2 %

End of Table 1

Lithotype	Sample	Description
Replacement variably-crystalline dolomites with relict silt-pelitic structure of the protolith, spotty ferruginized; or with an admixture (up to 35-40 %) of residual silt-sandy material	SL-6/5	Replacement variably-crystalline dolomite (crystal size from 0.03-0.05 to 0.15 mm), spotty due to uneven distribution of ferruginous (hematite?) matter, with a relict very fine-sandy-silt-pelitic structure. Consists of a variably-crystalline mass of dolomitic composition, with preservation of signs of the primary replaced rock. In the intercrystalline dolomitic space, clayey matter of pelitic structure is observed, along which dolomitization develops. A primary admixture (25 %) of very fine-sandy-silty material of predominantly micaceous-quartz composition is observed. Rare grains of orthoclase are noted. Poorly rounded lithoclasts of intraformational microgranular dolomites (intraclasts) sized 0.5-0.8 mm are present. Total Fsp content is 2.1 %
	SL-6/54	Ferruginized (hematite?) replacement dolomite, fine-crystalline, non-laminated, with abundant (30-35 %) fine- to very fine-sandy admixture of residual, poorly and semi-rounded grains of quartz (15-20 %), Fsp (10-12 %), single micas, rock fragments and dolomite lithoclasts (1-2 %). The groundmass of the rock consists of fine-crystalline dolomite. Dolomite crystals are subidiomorphic, coated with thin films of an iron-bearing mineral (hematite?), giving the rock a red tint. Many dolomite crystals have zonal, multi-stage structure with an initial non-idiomorphic nucleus in a thin film of iron oxides, a regeneration rim in a film, one or two growth zones separated by hematite films, up to idiomorphic dolomite crystals sized 0.1-0.2 mm. The rock preserves a residual (primary) fine- to very fine-grained, well-sorted admixture of poorly and semi-rounded grains in an amount of 30-35 %, among which quartz prevails (15-20 %). Individual quartz grains are regenerated with the formation of thin, discontinuous regeneration rims. Among Fsp, orthoclases predominate, single grains are regenerated; acid plagioclases are encountered. Micas (single) are represented by muscovite and biotite. Rock fragments are represented by microquartzites, acid effusives, dolomites (summarily 1-2 %). Dolomite lithoclasts are well-rounded, sized 0.2-1 mm. Total Fsp content is 9.4 %
	SL-6/22 SL-6/53	Replacement dolomite, analogous to SL-6/54. Contains an interlayer enriched in medium- to coarse-grained, well-sorted and rounded fragments (up to 40 % of the rock composition) of quartz, Fsp, and fragments of older rocks – gneisses, quartzites, acid effusives, ferruginous siliceous rocks, siderites. Among the lithoclasts, fragments of intraformational dolomites – microgranular and fine-crystalline, sometimes with bacterial structures – predominate. The rock of sample SL-6/53 is weakly sulfatized, contains single gypsum rosettes sized 0.2-0.5 mm. Total Fsp content is 4.5-13.1 %
Sandstones of various structural types and arkosic silt-sandstones with basal dolomitic cement	SL-6/51 SL-6/49	Fine- to very fine-grained sandstone, well-sorted, massive, arkosic. Composed of poorly and semi-rounded grains of quartz (50 %), Fsp (45 %), micas (5 %), lithoclasts (<1 %), with single glauconite, with basal (up to 40 %) fine-crystalline dolomitic cement. The rock contains an interlayer (up to 50 % of the thin section area) enriched in medium- to coarse-grained, well-sorted and rounded fragments of quartz, Fsp, gneisses, quartzites, acid effusives, ferruginous siliceous rocks, siderites; with a predominance of intraclasts of microgranular and fine-crystalline dolomites, locally with bacterial structures. In sample SL-6/51, coarse-sandy fragments are single. Total Fsp content is 14.7-21 %
	SL-6/20	Very fine-grained sandstone with abundant admixture of silty material (30-35 %), well-sorted, with con-sedimentary folds occurring between layers with undisturbed flaser-horizontal texture, arkosic. Composed of poorly and semi-rounded grains of quartz (60 %), Fsp (30 %), micas (10 %), single lithoclasts, with basal (up to 40 %) fine-crystalline dolomitic cement. Total Fsp content is 10.9 %

The position of the rocks in the section and their thin sections are shown in Fig.2.

The section extensively features red-brown dolomitic siltstones and dolomitic argillites, with green spots, less frequently green, thin-platy (in a dry state), sometimes loose and crumbly. Study of these terrigenous varieties in thin sections was not conducted, but they served as material for investigations of rare element content.

Geochemical Characteristics. *Correlation and clustering of elements.* The contents of rare elements are given in Table 2, contents of major oxides are provided in [3].

Journal of Mining Institute. *2025. Vol. 276. Iss. 2. P. 71-88*

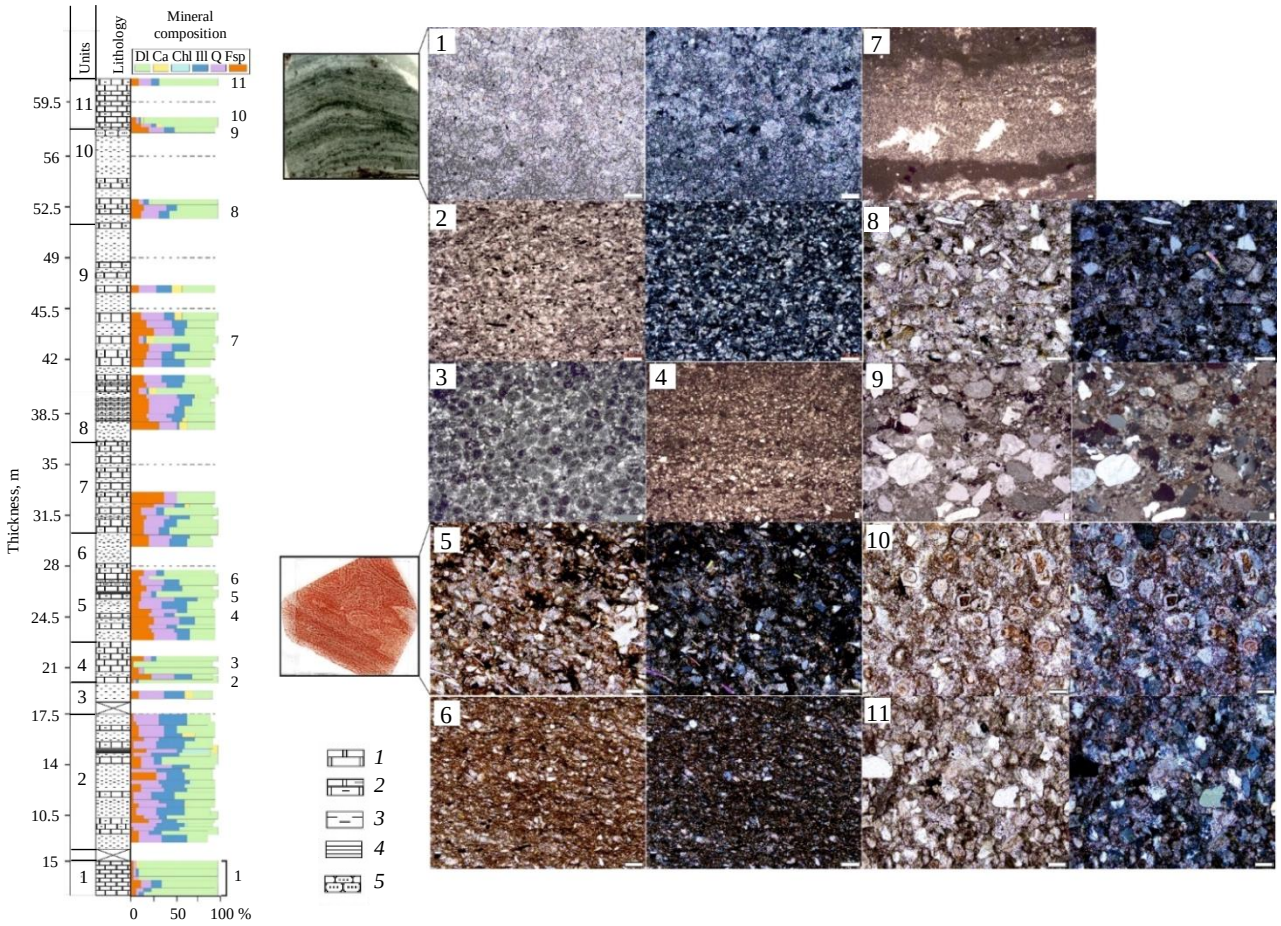

Fig.2. Section of the Lower Evenki Member on the Podkamennaya Tunguska River

Lithology column:
1 – dolomites; *2* – silty-clayey dolomites; *3* – dolomitic siltstones; *4* – dolomitic argillites; *5* – sandstones.
Normative mineral composition [3]:
Q – quartz, silica minerals; Fsp – feldspars; Ill – illite and micas; Chl – chlorite; Ca – calcite; Dl – dolomite.
Thin section photographs of samples:
1 – SL-1/1; 2 – SL-6/5; 3 – SL-6/8; 4 – SL-6/18; 5 – SL-6/20; 6 – SL-6/22; 7 – SL-6/43; 8 – SL-6/49; 9 – SL-6/51; 10 – SL-6/53; 11 – SL-6/54.
Scale bar 100 μm. For petrographic characteristics of samples, see Table 1

Table 2

Elemental composition of rocks from the Evenki Formation, ppm

Sample	Sampling point (from base of section), m	Li	Sc	Cr	Co	Ni	Cu	Zn	Rb	Sr	Ba	Pb	Th	U	Hf
SL-1/1	0.01	3.19	4.39	26.13	9.49	18.25	14.47	20.25	147.24	91.49	92.74	0.92	0.01	0.49	0.22
SL-1/5	0.67	26.00	8.39	63.17	15.33	30.29	23.05	32.77	165.87	166.92	439.71	1.58	2.13	0.80	2.26
SL-2/2	1.87	2.12	3.24	18.93	6.81	8.38	7.04	7.37	56.08	129.42	125.85	0.76	0.05	0.49	0.01
SL-3/1	1.53	1.70	3.01	14.71	4.97	6.20	3.00	7.78	6.08	216.64	700.54	0.84	0.07	0.08	0.03
SL-4/1	8.92	61.95	16.00	99.71	17.32	63.88	21.74	61.08	19.61	134.40	250.32	5.99	1.51	1.13	2.35
SL-4/2	9.47	26.75	9.37	77.12	12.33	24.18	8.70	25.81	291.35	131.66	259.23	1.90	2.92	0.62	3.13
SL-4/3	9.67	48.04	12.49	97.53	14.53	48.10	19.00	46.40	437.89	167.52	297.35	7.95	4.08	1.17	2.64
SL-4/4	9.92	59.79	14.55	97.90	16.85	58.27	20.02	57.20	385.28	207.81	358.74	9.02	4.30	1.39	4.68
SL-4/10	11.87	40.07	12.02	72.40	13.82	40.65	12.72	40.99	341.97	175.65	241.25	2.16	3.55	0.95	2.39
SL-5/3	12.92	53.59	17.08	101.93	16.09	53.39	19.54	54.00	34.57	91.95	299.26	5.21	3.20	0.95	2.61
SL-5/7	14.32	8.42	8.00	50.30	12.88	22.12	7.43	25.24	174.57	124.38	82.04	2.09	0.25	1.14	1.68
SL-5/9	15.02	58.98	14.00	118.66	17.51	62.90	22.95	66.24	122.39	126.50	255.86	10.12	2.03	1.42	5.86
SL-5/11	15.72	73.09	12.96	117.93	18.69	76.27	25.00	82.27	35.97	156.24	319.97	7.10	1.28	1.57	4.87
SL-6/2	16.77	58.15	13.05	104.51	16.99	60.94	20.42	63.04	209.90	607.03	286.38	8.49	3.11	1.31	4.88
SL-6/4	19.17	30.19	12.74	111.50	14.34	38.04	17.31	35.98	185.56	232.24	350.70	5.97	2.51	0.92	4.07
SL-6/5	20.22	1.50	3.56	14.07	5.80	8.07	10.24	11.37	88.43	72.66	12.91	0.75	0.04	0.46	0.04
SL-6/6	20.57	42.00	15.70	85.86	13.95	39.70	20.32	45.42	36.51	456.51	338.05	3.19	2.24	0.89	1.84
SL-6/9	21.62	7.74	9.20	48.30	14.60	16.46	18.36	20.76	18.44	110.11	140.01	0.86	0.07	0.53	0.47
SL-6/13	24.42	33.61	12.40	147.34	12.03	38.33	13.40	40.86	247.50	68.88	302.45	2.48	2.33	1.09	5.11

End of Table 2

Sample	Sampling point (from base of section), m	Li	Sc	Cr	Co	Ni	Cu	Zn	Rb	Sr	Ba	Pb	Th	U	Hf
SL-6/17	25.82	37.19	12.56	108.61	12.54	40.32	14.24	42.92	203.93	80.08	325.81	2.83	1.97	0.87	3.62
SL-6/18	26.17	5.43	6.70	44.68	11.59	16.75	6.51	19.92	193.01	88.07	114.24	1.09	0.03	0.71	0.74
SL-6/19	26.52	53.34	11.77	106.33	16.15	51.38	17.34	56.58	273.43	80.77	319.80	2.10	4.22	1.32	4.85
SL-6/20	26.87	23.32	12.19	128.86	10.23	23.52	9.76	24.32	250.45	50.20	227.69	2.36	2.69	0.91	2.59
SL-6/24	30.02	45.93	11.91	109.22	13.96	48.28	16.27	45.55	206.12	74.04	291.90	4.02	2.84	1.17	4.39
SL-6/29	32.17	30.44	16.45	91.34	16.17	31.37	12.46	33.00	40.28	95.34	268.23	2.24	2.15	0.59	2.11
SL-6/34	38.77	24.02	11.87	103.88	12.58	28.22	10.55	26.89	380.10	74.62	269.23	2.16	2.93	0.97	2.37
SL-6/35	39.32	20.74	12.71	114.08	13.62	39.03	11.71	35.79	219.44	76.28	237.78	3.06	1.73	0.92	3.49
SL-6/36	39.67	28.49	11.52	110.00	13.12	39.67	11.52	36.94	92.55	67.36	263.54	1.97	1.00	1.04	2.67
SL-6/39	40.87	39.17	11.14	104.59	15.68	49.61	13.37	41.98	308.93	90.88	327.08	3.25	2.98	1.19	3.51
SL-6/41	42.47	24.13	10.80	82.85	13.87	34.13	10.60	31.73	222.74	94.48	238.43	2.43	2.13	4.91	2.98
SL-6/42	43.02	28.80	10.86	87.89	12.35	41.69	11.65	38.90	247.42	64.25	275.80	3.00	2.33	0.96	3.37
SL-6/45	44.47	23.74	11.48	93.35	12.17	38.63	9.33	29.87	255.29	78.39	294.20	1.99	2.66	0.95	3.79
SL-6/48	51.92	11.55	7.06	60.76	7.77	16.57	5.61	15.68	166.17	38.17	208.56	1.22	1.15	0.76	0.83
SL-6/49	52.47	8.90	8.45	108.24	9.07	18.25	7.60	15.26	129.22	59.64	159.11	1.78	0.91	0.73	2.22
SL-6/51	57.87	16.42	9.85	73.17	11.40	23.51	10.77	22.03	158.86	77.25	562.44	2.07	0.94	0.87	1.99
SL-6/54	61	11.42	7.41	58.23	7.70	12.07	4.57	11.50	193.18	55.71	172.27	1.60	1.78	0.76	0.84

Sample	La	Ce	Pr	Nd	Sm	Eu	Gd	Tb	Dy	Ho	Er	Yb	Lu	Ce/Ce*	Eu/Eu*
SL-1/1	0.25	0.41	0.06	0.21	0.04	0.07	0.05	0.03	0.14	0.02	0.02	0.10	0.03	0.77	6.63
SL-1/5	4.94	10.16	1.37	5.05	1.00	1.29	1.02	0.68	3.44	0.62	1.85	1.43	0.20	0.89	5.99
SL-2/2	0.23	0.38	0.06	0.23	0.04	0.07	0.05	0.04	0.06	0.00	0.07	0.15	0.03	0.71	7.80
SL-3/1	0.05	0.10	0.10	0.10	0.10	0.10	0.10	0.04	0.08	0.10	0.08	0.09	0.08	0.21	4.93
SL-4/1	6.07	16.91	2.02	8.83	1.89	0.46	1.99	0.34	1.84	0.28	1.10	1.00	0.08	1.08	0.58
SL-4/2	6.99	14.73	1.94	7.39	1.70	2.11	1.69	1.34	6.78	1.30	3.75	3.15	0.47	0.91	2.60
SL-4/3	7.26	13.87	1.76	6.42	1.26	1.51	1.28	0.91	4.76	0.92	2.82	2.47	0.37	0.88	1.89
SL-4/4	6.45	13.55	1.76	6.60	1.33	1.62	1.38	1.00	5.29	1.04	3.14	2.84	0.43	0.91	2.05
SL-4/10	6.48	13.58	1.79	6.72	1.43	1.77	1.46	1.15	5.88	1.15	3.28	2.74	0.40	0.91	2.22
SL-5/3	10.28	23.28	2.63	11.12	2.30	0.55	2.49	0.41	2.10	0.33	1.25	1.12	0.10	1.02	0.71
SL-5/7	2.70	4.69	0.76	2.86	0.57	0.69	0.56	0.35	1.85	0.32	0.84	0.55	0.07	0.74	5.73
SL-5/9	1.80	5.09	0.66	2.65	0.67	0.74	0.69	0.60	3.87	0.79	2.49	2.45	0.34	1.04	0.93
SL-5/11	2.09	5.37	0.78	3.21	0.72	0.91	0.71	0.52	3.14	0.65	2.00	1.95	0.30	0.93	1.11
SL-6/2	4.13	9.69	1.29	4.96	1.11	1.40	1.12	0.91	5.01	1.01	3.01	2.71	0.40	0.95	1.74
SL-6/4	7.15	27.99	4.78	18.57	2.80	2.84	2.50	1.45	5.30	0.97	3.07	2.23	0.33	0.96	3.32
SL-6/5	0.13	0.21	0.08	0.13	0.07	0.01	0.07	0.06	0.01	0.01	0.09	0.16	0.03	0.41	0.45
SL-6/6	8.75	20.01	2.27	9.58	1.91	0.47	2.08	0.33	1.68	0.24	0.94	0.83	0.05	1.02	0.61
SL-6/9	2.47	4.90	0.70	3.13	0.51	0.10	0.58	0.06	0.35	0.02	0.14	0.08	0.06	0.84	0.87
SL-6/13	4.49	10.23	1.28	4.74	0.95	1.04	0.93	0.62	3.33	0.63	1.84	1.52	0.22	0.97	1.28
SL-6/17	2.94	7.60	1.02	3.91	0.86	1.04	0.85	0.63	3.59	0.71	2.09	1.84	0.27	0.98	1.28
SL-6/18	0.52	0.99	0.13	0.43	0.08	0.11	0.10	0.01	0.23	0.04	0.03	0.04	0.02	0.86	5.61
SL-6/19	7.56	14.01	1.76	6.36	1.20	1.41	1.25	0.85	4.24	0.84	2.51	2.02	0.30	0.88	1.77
SL-6/20	4.41	9.30	1.28	4.71	1.00	1.17	1.03	0.75	3.98	0.75	2.12	1.71	0.24	0.89	1.47
SL-6/24	4.76	10.17	1.34	5.01	1.11	1.34	1.11	0.86	4.74	0.93	2.70	2.40	0.36	0.91	1.66
SL-6/29	17.09	52.06	7.85	32.80	5.11	1.13	4.80	0.65	2.34	0.35	1.37	1.01	0.08	0.97	1.36
SL-6/34	5.73	12.70	1.82	6.71	1.33	1.57	1.33	0.97	4.83	0.92	2.70	2.21	0.32	0.89	1.94
SL-6/35	2.97	8.13	1.10	3.96	0.68	0.74	0.67	0.34	1.62	0.36	0.85	0.56	0.08	1.00	0.91
SL-6/36	2.56	6.65	1.07	4.10	0.91	1.06	0.88	0.63	3.50	0.68	1.99	1.62	0.24	0.88	1.28
SL-6/39	8.52	15.77	2.15	7.90	1.61	1.86	1.57	1.16	5.85	1.19	3.21	2.59	0.37	0.84	2.27
SL-6/41	5.81	12.24	1.75	6.42	1.31	1.59	1.59	0.95	4.84	0.88	2.48	1.84	0.25	0.87	2.17
SL-6/42	5.22	10.95	1.38	5.16	1.04	1.23	1.01	0.73	3.84	0.72	2.00	1.59	0.22	0.93	1.50
SL-6/45	5.55	11.48	1.65	6.12	1.19	1.36	1.17	0.80	4.04	0.74	2.10	1.63	0.25	0.86	1.67
SL-6/48	2.25	3.61	0.75	2.79	0.53	0.69	0.55	0.33	2.01	0.35	0.91	0.66	0.09	0.63	6.03
SL-6/49	1.99	4.73	0.65	2.41	0.52	0.64	0.52	0.33	1.94	0.35	0.89	0.59	0.08	0.94	5.83
SL-6/51	2.17	4.38	0.58	2.08	0.43	0.67	0.52	0.27	1.66	0.27	0.77	0.58	0.07	0.89	6.68
SL-6/54	4.68	7.84	1.33	5.02	1.04	1.29	1.04	0.77	3.98	0.74	2.06	1.48	0.21	0.71	5.83

Note. Blue highlighting indicates carbonate rocks (based on thin section study); Eu/Eu* = $[Eu_{UCC}/(Sm_{UCC}*Gd_{UCC})^{0.5}]$; $(Ce/Ce^*)_{UCC}$ = $= [2Ce_{UCC}/(La_{UCC} + Pr_{UCC})]$.

For the analysis and visualization of statistical data, a heat map with complete-linkage clustering was constructed (Fig.3). The color indicates the magnitude of the *z*-score for each sample for a given element. The parameter *z*-score (standardized score) provides an idea of how far a value in a

Journal of Mining Institute. 2025. Vol. 276. Iss. 2. P. 71-88

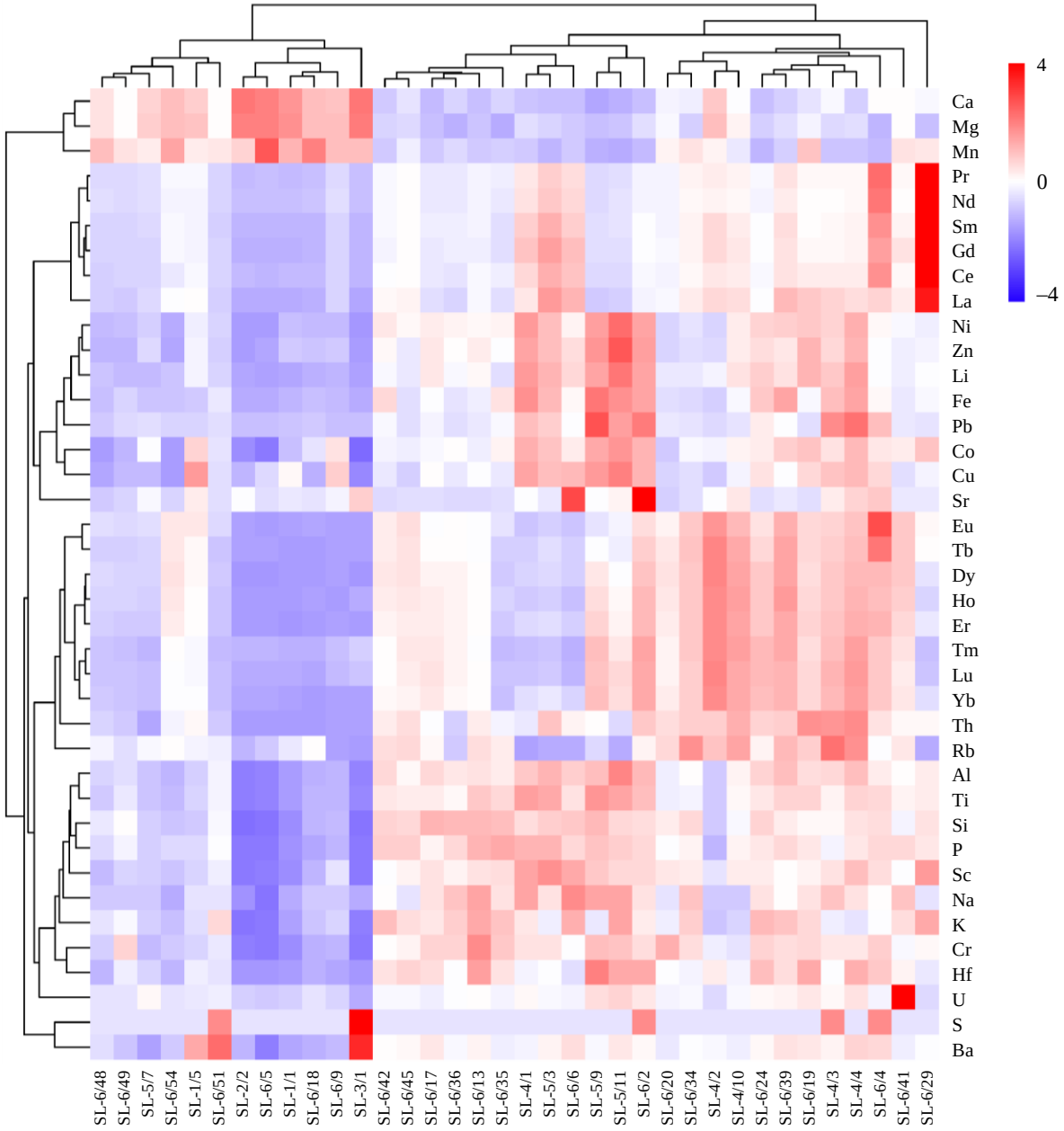

Fig.3. Heat map of the chemical composition of the studied rocks of the Lower Evenki Member, Podkamennaya Tunguska River

data point is from the mean. To calculate the *z*-score, besides the value for each individual sample, the mean value μ and the standard deviation σ of the population are used. The sign of the *z*-score indicates which half of the distribution the indicator falls into – a positive sign (or its absence) indicates that the indicator is above the mean and is in the right part of the distribution, a negative sign means that the score is below the mean value and is in the left part of the distribution. The magnitude of the obtained number in units of standard deviations shows how far the score is from the center or mean value. The less saturated the color shade in a point and the closer the score value is to zero, the closer the value is to the sample mean. Sample composition: dolomites with stromatolitic texture (three samples), clotted-peloidal dolomites (two samples), replacement crystalline dolomites without preservation of primary protolith structures (one sample), replacement variably-crystalline dolomites with relict silt-pelitic structure of the protolith (two samples), dolomitic argillites and dolomitic siltstones (23 samples), sandstones and arkosic silt-sandstones with basal dolomitic

cement (five samples). The heat map clearly visually identifies the presence of anomalies within the sample – values exceeding the sample mean for a given chemical element.

The considered elements in the rocks can be grouped as follows:

• Group 1 – Ca, Mg, Mn. Associated with their presence in dolomite (Mn is a characteristic isomorphic admixture).

• Group 2 – LREE, except Eu + Gd, Ni, Zn, Li, Fe, Pb, Co, Cu, Sr.

• Group 3 – HREE + Eu, Th, Rb, Al, Ti, Si, P, Sc, Na, K, Cr, Hf, U.

The concentrations of elements in groups 2 and 3 depend on the amount and composition of the terrigenous component, which is also expressed in the negative correlation between elements of group 1 and groups 2, 3.

• Group 4 – S, Ba. Elevated contents in individual samples likely indicate the presence of barite in them.

In addition to the grouping of elements, it is important to pay attention to the clustering of samples. Depending on the variations in dolomite content and terrigenous component, two groups of samples are distinguished. The first group includes both dolomites and sandstones, arkosic silt-sandstones with basal dolomitic cement (SL-6/48, SL-6/49, SL-6/51), the second group includes siltstones, argillites, and sandstones. Further normalization against a standard should be performed based on this division, using clarke values for either carbonate or clayey and sandy rocks.

Isotopic composition of carbon and oxygen in carbonates ($\delta^{13}C$, $\delta^{18}O$). The $\delta^{13}C$, $\delta^{18}O$ values in the samples are given in Table 3 and Fig.4. The analyzed rocks are characterized by variations in $\delta^{13}C$ from –1.4 to –0.3 ‰ and $\delta^{18}O$ from –7.3 to –5.7 ‰. In chemostratigraphy of the Late Proterozoic and Early Paleozoic, the oxygen isotopic composition is indicative as a marker of post-sedimentary alterations and the preservation of the C-isotope system. For limestones, it has been empirically established that during diagenetic and later alterations, the concentrations of Mn and Fe in them increase, while the Sr content decreases; therefore, the following criteria are used to determine the preservation of the C-isotope system – Mn/Sr ≤ 4, Fe/Sr ≤ 10, $\delta^{18}O \geq -10$ ‰ VPDB [16-18]. For dolomites, different criteria have been proposed – Mn/Sr ≤ 6, Fe/Sr ≤ 15 [17, 19].

Table 3

Isotopic composition of C and O of dolomites from the Lower Evenki Member

Sample	Lithotype	$\delta^{13}C$ (VPDB), ‰	$\delta^{18}O$ (VPDB), ‰	Sample	Lithotype	$\delta^{13}C$ (VPDB), ‰	$\delta^{18}O$ (VPDB), ‰
SL-1/3	1	–1.4	–7.2	SL-6/5	4	–0.9	–6.1
SL-1/6	1	–1.2	–6.9	SL-6/21	4	–0.4	–6.5
SL-3/1	1	–0.3	–6.9	SL-6/22	4	–0.3	–6.4
SL-6/43	1	–1.4	–7.3	SL-6/28	4	–0.5	–6.3
SL-2/1	2	–1.1	–7.0	SL-6/50	4	–1.1	–6.3
SL-2/2	2	–1.2	–6.8	SL-6/53	4	–1.4	–6.3
SL-6/8	3	–0.8	–6.5	SL-6/54	4	–0.7	–5.7
SL-6/18	3	–0.5	–6.5				

Note. Lithotypes: 1 – stromatolitic dolomites; 2 – replacement crystalline dolomites without preservation of primary protolith structures; 3 – clotted-peloidal dolomites; 4 – replacement variably-crystalline dolomites with relict silt-pelitic structure of the protolith.

Dolomites with stromatolitic texture are characterized by Mn/Sr values from 5 to 12.5, Fe/Sr from 16.8 to 70; the replacement crystalline dolomite without preservation of primary protolith structures has Mn/Sr = 7.8, Fe/Sr = 23.2. The ratios in clotted-peloidal dolomites for Mn/Sr are 9.8-15.2, for Fe/Sr – 69.2-100.1; in replacement variably-crystalline dolomites with relict silt-pelitic structure of the protolith – Mn/Sr 20.6-21.3, Fe/Sr 49.1-180.8. For the studied dolomites of the Lower Evenki Member, these Sr ratios with other elements are not very informative due to the high content of aluminosilicate clastics (clays, micas, Fsp, containing Sr as an impurity and accumulating radiogenic Sr).

Journal of Mining Institute. 2025. Vol. 276. Iss. 2. P. 71-88

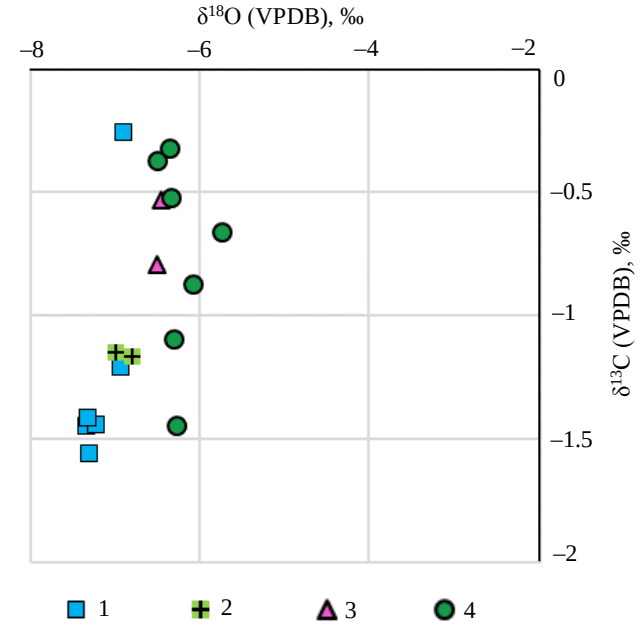

Fig.4. Plot of $\delta^{18}O$-$\delta^{13}C$ values for dolomites of the Lower Evenki Member

1 – stromatolitic; 2 – replacement crystalline without preservation of primary protolith structures; 3 – clotted-peloidal; 4 – replacement variably-crystalline with relict silt-pelitic structure of the protolith

On the $\delta^{18}O$-$\delta^{13}C$ plot (Fig.4) the composition points of the four described dolomite types do not form separate clusters, but a similar isotopic composition is noted for dolomites with stromatolitic texture and replacement crystalline dolomites without preservation of primary protolith structures. For these two types, $\delta^{18}O$ ranges from –6.8 to –7.3 ‰. Sample SL-3/1 stands out in terms of $\delta^{13}C$; for the other dolomites of these groups, this parameter ranges from –1.4 to –1.1 ‰. Replacement variably-crystalline dolomites with relict silt-pelitic structure of the protolith are distinguished by relatively wide variations in $\delta^{13}C$ – from –1.4 to –0.3 ‰. Clotted-peloidal dolomites occupy an intermediate position on the diagram.

The $\delta^{13}C$ values in the samples of the Evenki Formation dolomites lie within the recorded range of $\delta^{13}C$ values for Cambrian sedimentary carbonates from –2.5 to 2 ‰ PDB [20, 21], but the preservation of the isotopic system is debatable. Thus, despite signs of diagenesis, hypergenesis, and other post-sedimentary alterations, the isotopic composition of carbon and oxygen generally corresponds to the summary curves of the evolution of the C and O isotopic composition for marine carbonate rocks of the Cambrian.

Discussion

Genetic interpretation of the identified lithology types. Among the genetic features of the identified types, the widespread development of dolomites with stromatolitic texture and/or bacterial structures (remains of calcimicrobes *Renalcis*, micro-oncolites, katagraphs, clots, peloids) is noted. In certain types, signs of subaerial exposure of the sediment are present in the form of weakly expressed microkarst (SL-1/6 (see Fig.2, thin section 1), SL-6/43 (see Fig.2, thin section 7), as well as fenestral structures typical of tidal flat settings (SL-6/43). In the carbonate-terrigenous varieties, variations in the granulometric composition of the silt-sandy component and its distribution along laminae are observed (SL-6/18 (see Fig.2, thin section 4), enrichment of individual layers with medium- to coarse-sandy aluminosilicate clastic material (SL-6/51 (see Fig.2, thin section 9) or very fine-sandy-silty micaceous material (SL-6/54 (see Fig.2, thin section 11), the presence of poorly expressed cross and graded bedding, flaser-horizontal texture, as well as con-sedimentary deformations (SL-6/20 (see Fig.2, thin section 5), indicating variations in the hydrodynamic regime and sedimentation mode, increased input of terrigenous material or its redistribution within the sedimentation basin. In the upper part of the section (SL-6/49, SL-6/53 (see Fig.2, thin sections 8, 10), gypsum is detected. The depositional settings are reconstructed as sublittoral, littoral (tidal flat), and possibly sabkha (in the upper part of the section).

Post-sedimentary alterations of the rocks are associated with multi-stage dolomitization processes – early, syngenetic, observed in types of dolomites with stromatolitic texture and/or bacterial structures, and later, identified by the authors in types of replacement dolomites and silt-sandstones with dolomitic cement. In the first case, dolomite is generated and precipitated in alkaline conditions of syngenesis – early diagenesis, caused by the activity of lower organisms; such a mechanism of

dolomite formation is described in detail in [22-24]. In the second case, the dolomites have a variably-crystalline structure, and in some samples, signs of the replaced rock are absent (SL-2/2). In samples SL-6/5, SL-6/22, SL-6/53, SL-6/54, a silt-pelitic primary structure and an admixture of sandy material are noted. The newly formed dolomite is massive, unevenly distributed in different areas. The crystals are subidiomorphic, zonal, with one to three growth zones separated by films of an iron-bearing mineral (hematite?), reflecting several stages of crystallization. In sandstones and silt-sandstones with basal dolomitic cement (SL-6/20, SL-6/49, SL-6/51), the structural features of the secondary dolomite are similar; in rare cases, corrosion of silicate fragments by dolomite crystals is observed.

Geochemistry of dolomites. The REE content in dolomites can provide information about the composition of the dolomitizing fluid. The significant role of oceanic aqueous solutions, probably enriched with ore substances from hydrothermal fluids, has been established for the formation of the Neoarchean Malmani dolomites of the manganese occurrence in the Haifeldav region of the North-West Province, South Africa [25, 26]. The study of REE contents in manganese nodules and the underlying Malmani dolomites allowed the authors to trace their close genetic relationship and substantiate a genetic model of the multifactorial process of manganese ore genesis in the studied territory [25, 26].

It has been established that the REE distribution in primary dolomites is inherited mainly from seawater and/or marine brines and does not change relative to the preceding paragenetic limestones [27]. Dolomites altered by meteoric waters or hydrothermal solutions should have a REE distribution different from that of seawater [28-30].

Along with traditional normalization to NASC or PAAS, normalization of dolomites to the composition of modern seawater is justified [30, 31]. The recrystallization process can lead to changes in total REE concentrations but does not alter the overall REE distribution, including enrichment in Ce_{SN} (SN – seawater normalized) and LREE [30]. However, the influence of meteoric waters can lead to a change in the magnitude of the Ce anomaly, and the impact of hydrothermal fluids is reflected in complex fluctuations on the REE spider diagram and in the emergence of a positive Eu anomaly [30].

The composition of the Evenki Formation dolomites was normalized to modern seawater [32] and PAAS [33], the spectra are shown in Fig.5. The dolomites have a pronounced positive Ce anomaly when normalized to seawater composition. Low Ce contents in the modern ocean can in some cases lead to positive Ce anomalies in seawater-normalized spectra [30]. To verify whether a positive Ce anomaly truly exists, the following method is used [34]: $(Pr/Pr^*)_{SN}$ $[2Pr_{SN}/(Ce_{SN} + Nd_{SN})]$ is calculated and compared with $(Ce/Ce^*)_{SN}$ $[2Ce_{SN}/(La_{SN} + Pr_{SN})]$, where SN denotes seawater. If $(Pr/Pr^*)_{SN} < 1$, then a positive Ce_{SN} anomaly exists; if $(Pr/Pr^*)_{SN} > 1$, a negative Ce_{SN} anomaly exists. For the studied dolomites $(Ce/Ce^*)_{SN}$ varies from 2.0 to 10.3 (average 7.7), $(Pr/Pr^*)_{SN}$ = 0.24-0.69, except for sample SL-3/1, where $(Pr/Pr^*)_{SN}$ =1.56. For the stromatolitic dolomite SL-3/1, a negative Ce anomaly was identified, and it can be assumed that its formation was influenced by meteoric waters. The cerium anomaly in this sample could also be a consequence of sedimentation in more oxygen-rich settings. When normalized to the upper crust (calculating $(Ce/Ce^*)_{UCC} = [2Ce_{UCC}/(La_{UCC} + Pr_{UCC})]$, where UCC is the upper continental crust [35]), a negative Ce anomaly is observed – 0.21-0.89.

The Nd_{SN}/Yb_{SN} ratio varies from 0.3 to 15.07, indicating LREE enrichment due to the terrigenous admixture. The ratio of non-normalized ΣLREE to ΣHREE contents in the dolomites ranges from 0.82 (SL-3/1) to 8.72. It was previously established [36], that in carbonate rocks of the southern folded framing of the Siberian Platform, the proportion of LREE increases with an increasing share of clastic material, and with its decrease, the total REE content drops, but the proportion of HREE increases.

Journal of Mining Institute. 2025. Vol. 276. Iss. 2. P. 71-88

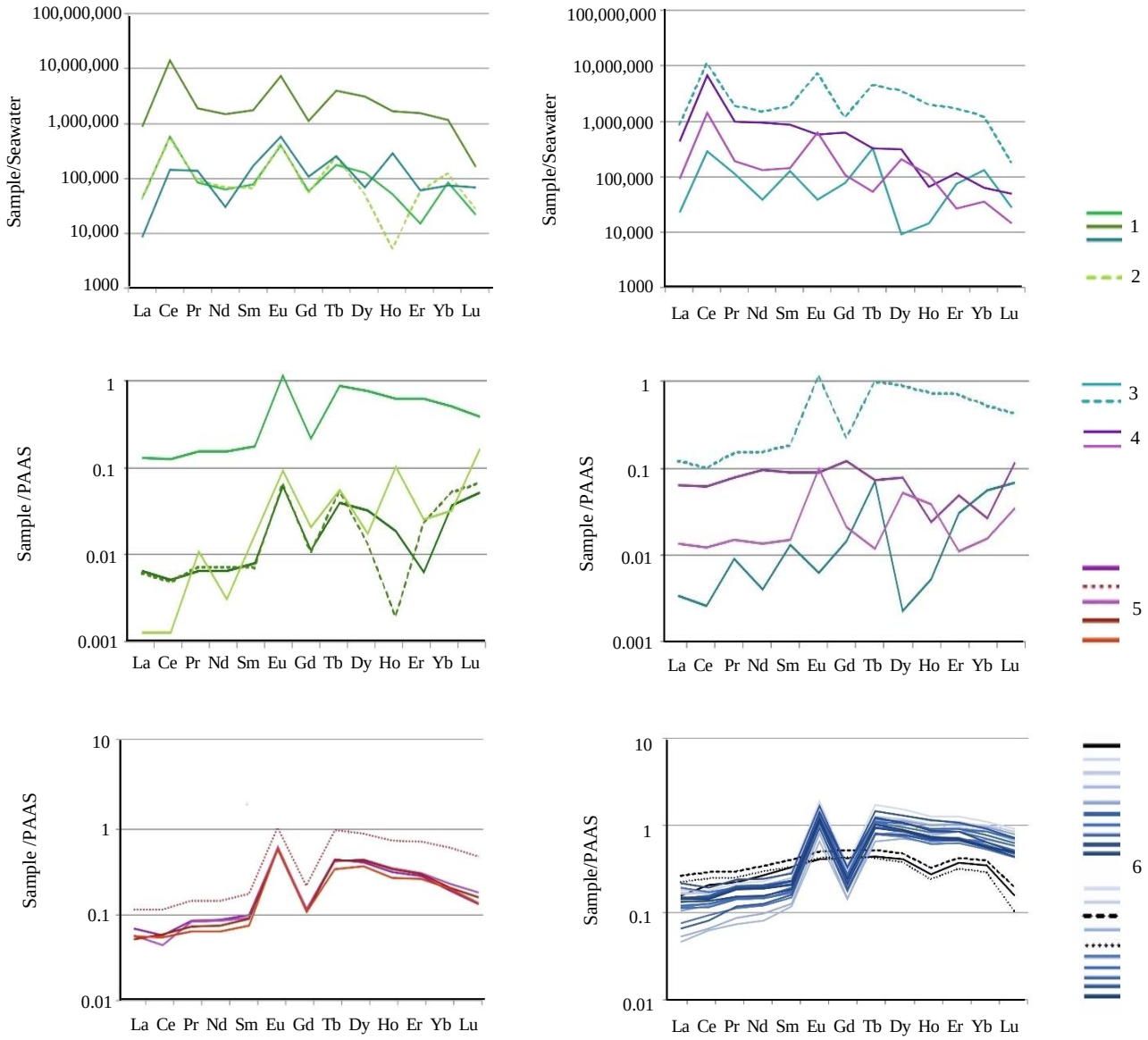

Fig.5. REE distribution spider diagrams for rocks of the Lower Evenki Member

1 – dolomites with stromatolitic texture; 2 – replacement crystalline dolomites without preservation of primary protolith structures; 3 – clotted-peloidal dolomites; 4 – replacement variably-crystalline dolomites with relict silt-pelitic structure of the protolith; 5 – sandstones and arkosic silt-sandstones with basal dolomitic cement; 6 – dolomitic argillites and dolomitic siltstones. Normalizing values: seawater after [32], PAAS – [33]

When normalized to modern seawater and chondrite concentrations, a pronounced positive Eu anomaly is observed, with the exception of samples SL-6/5 and SL-6/9, which have a negative Eu anomaly. When normalized to the upper continental crust composition, the $Eu/Eu^* = [Eu_{UCC}/(Sm_{UCC}*Gd_{UCC})^{0.5}]$ value is 0.45 and 0.87 for samples SL-6/5 and SL-6/9, respectively, and for the other studied dolomites – 4.93-6.63. In contrast, Early Paleozoic carbonate deposits of the shelf framing the Siberian Platform are characterized by a pronounced negative Eu anomaly [36, 37]. The reasons for such enrichment of carbonates in europium warrant detailed consideration.

Europium can be incorporated into the calcite crystal lattice [38, 39]. Researchers attribute positive Eu_{CN} (CN – chondrite-normalized) anomalies in dolomite veins to the composition of the primary fluid [40]. Leachates with positive Eu anomalies can form as a result of preliminary mobilization of Eu during high-temperature (>200 °C) alteration processes of rocks containing Ca-plagioclases, when Eu^{3+} is reduced to Eu^{2+} [41]. Eu^{2+}, adsorbed on mineral surfaces and in intercrystalline

space, becomes readily available for remobilization in the aqueous environment after cooling and thermochemical oxidation to Eu^{3+} [41, 42]. Thus, europium enrichment is often considered an indicator of the influence of hydrothermal fluids on the sedimentary system.

Besides reducing conditions during diagenesis and the influence of fluids with high Eu content, a positive anomaly in bulk samples can be a consequence of the contribution of clastic admixture. For carbonate rocks with significant terrigenous admixture, when normalized to shale, "smoothed" spectra without pronounced anomalies are often characteristic, and the REE sum correlates with the insoluble residue [43, 44]. Such features are observed for Riphean – Vendian carbonate rocks of the Baykit Anteclise [44], and among the studied samples, there are carbonates with a Eu anomaly. The author of [44] following the authors of [40] associates its origin either with reducing formation conditions or with the presence of Ca-plagioclases in the rocks.

When normalizing the dolomites of the Lower Evenki Member to PAAS (Fig.5) a positive Eu anomaly (except for SL-6/9) is also distinguished. At the same time, the dolomites with stromatolitic texture (Eu/Eu* = 4.9-6.6) contain a finely dispersed admixture of Fsp and micas. In the replacement crystalline dolomite (SL-2/2, Eu/Eu* = 7.8), residual grains of muscovite and plagioclase are observed. Micas and plagioclases often contain Eu impurities. The highest correlation coefficient (considering only the carbonate rock sample set) links Eu with Li (0.83) and Th (0.95), as well as with other LREE. The emergence of the positive Eu anomaly is likely related to Eu-bearing minerals in the terrigenous component of the dolomites and mixed rocks, rather than to hydrothermal solutions. At the same time, no direct correlation is observed between the REE content and the amount of terrigenous admixture; therefore, the influence of reducing conditions or the composition of the dolomitizing solution on the REE distribution in the dolomites cannot be ruled out.

Relative to the Clarke values for carbonate rocks [45], the studied deposits are noticeably enriched in Co, Cr, Sc, Rb and depleted in Cu, Zn, Li, Ba (except for sample SL-1/5, which is enriched in these elements), as well as Pb and Sr (Fig.6, *a*). Primarily, the relative variations in depletion/enrichment characterize the elemental composition of the terrigenous admixture. Due to the presence of up to 40 % dolomitic cement in the sandstones and their location in the same cluster with the dolomites, samples SL-6/51 and SL-6/49 were also normalized against carbonate rocks.

Geochemistry of carbonate-terrigenous rocks. When normalized to PAAS, the dolomitic argillites, dolomitic siltstones, sandstones, and silt-sandstones (see Fig.5) are generally characterized by enrichment in HREE relative to LREE (except for Eu). In samples SL-4/1, SL-5/3, SL-6/6, SL-6/29, conversely, enrichment in LREE relative to HREE is observed.

Similarly to the carbonate rocks, a positive Eu anomaly was identified, except for samples SL-4/1, SL-5/3, SL-6/6, SL-6/29. When normalized to the upper continental crust composition, the Eu/Eu* value for dolomitic argillites and dolomitic siltstones ranges from 0.58 (SL-4/1) to 3.32 (SL-6/4), averaging 1.6. The Ce/Ce* value varies from 0.84 to 1.08. The total REE content ranges from 22.1 (SL-6/35) to 126.7 (SL-6/29) ppm. The ratio of non-normalized ΣLREE to ΣHREE contents ranges from 1 (SL-5/9) to 10.89 (SL-6/29), average 3.06.

For sandstones and silt-sandstones, when normalized to the upper continental crust composition, the Eu/Eu* value is within 5.73-6.68, and Ce/Ce* – 0.63-0.94. The total REE content ranges from 14.5 to 16.85 ppm. The ratio of non-normalized LREE to HREE contents ranges from 2.13 to 2.68 (the LREE sum increases due to Eu).

Relative to the Clarke values for clays and clay shales [45], the studied rocks are depleted in Cu, Zn, Pb, Ba, Th, U, similar to the described carbonate lithological types, except for sample SL-6/41, which is weakly enriched in uranium. Significant enrichment of individual samples in Rb and Sr is observed, while the concentrations of Co, Ni, Cr, Sc are close to the Clarke values with minor depletion or enrichment in these elements (Fig.6, *b*).

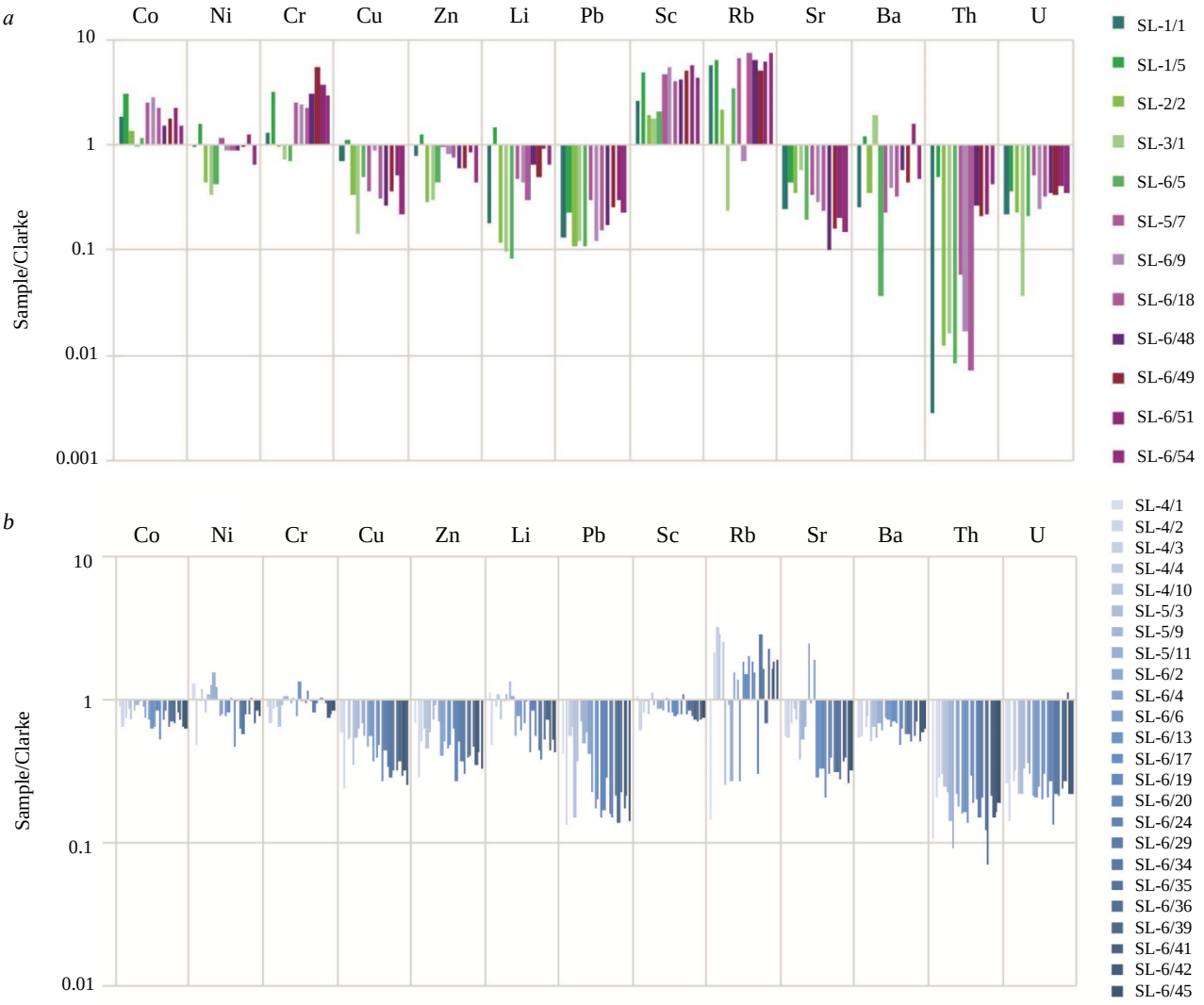

Fig.6. Clarke-normalized concentrations of trace elements: *a* – carbonate rocks (Clarke for carbonate rocks [45]); *b* – in carbonate-terrigenous rocks of the Evenki Formation (Clarke for clays and clay shales [45])

The Hf-La/Th plot [46] allows distinguishing the compositional fields of sedimentary formations formed by the erosion of oceanic islands composed of tholeitic basalts A, andesites B, or acid volcanics C, and also shows areas of mixing of clastics from these rock types D (Fig.7, *a*). In Fig.7, *a* the composition points of the carbonate-terrigenous rocks of the Evenki Formation fall within the field of felsic sources. Sample SL-6/29 stands out, falling into the field of formations formed by the erosion of island arcs with a predominance of andesites. This sample is characterized by the highest LREE/HREE ratio and total REE content in the sample set. Sample SL-5/7 falls into the field of formations formed by the erosion of oceanic islands with a predominance of tholeitic basalts. On the La/Sc-Th/Co plot [47] (Fig.7, *b*), the composition of the Evenki Formation rocks demonstrates a mixed source – products of the erosion of rocks of both acidic E and basic F composition.

A complex of volcanogenic-sedimentary rocks, similar in composition to modern ensialic island arcs, including rocks of the calc-alkaline rhyolite-andesite-basalt volcanic series, constitutes the terranes in the northwestern part of the Yenisei Ridge [48, 49]. Furthermore, Precambrian metasedimentary formations are widespread in the adjacent regions of the Yenisei Ridge – within the Central-Angara (whose sequences correspond to deposits of passive continental margins [48]) and Isakov terranes, which most likely acted as suppliers of clastic material. Thin sections contain fragments of gneisses, quartzites, acid effusives, ferruginous siliceous rocks, and siderites.

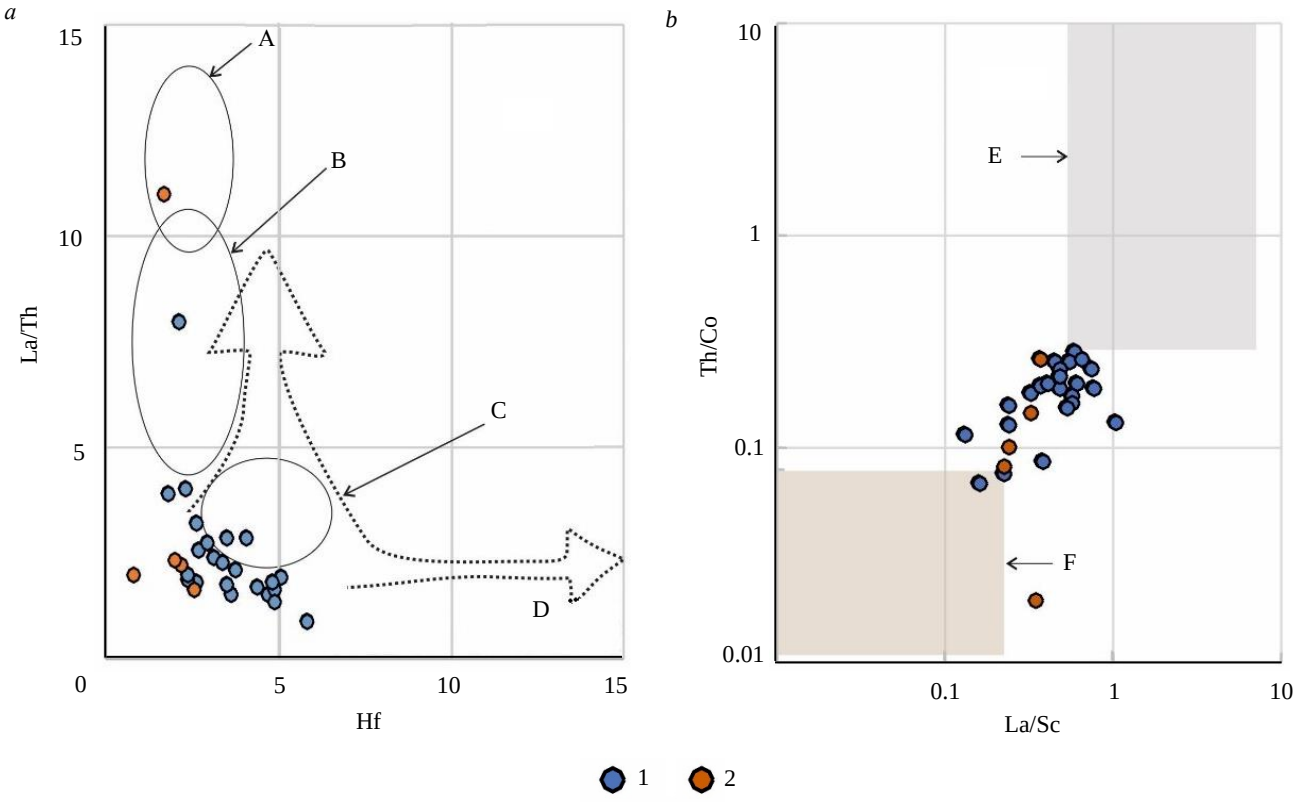

Fig.7. Position of rocks on plots: *a* – Hf-La/Th [46]; *b* – La/Sc-Th/Co [47]

1 – dolomitic siltstones and dolomitic argillites;
2 – sandstones and arkosic silt-sandstones with basal dolomitic cement

Previously, researchers obtained ages of detrital zircon grains dZr from rocks of the Evenki Formation in the East Angara zone (north of the Yenisei Ridge) [50, 51]. It was established [50, 51], that the Evenki Formation contains significant amounts of erosion products from Neoproterozoic crystalline complexes, which was not recorded in older strata, whose source was predominantly the Archean-Palaeoproterozoic crystalline complexes of the Siberian Platform basement. The sandstones of the Evenki Formation contain products of the erosion of Neoproterozoic-Cambrian crystalline complexes formed during the corresponding stages of evolution of the structural elements of the Central Asian Fold Belt conjugated with the Siberian Platform.

Conclusion

As a result of the conducted research, the lithological features of the sublittoral-littoral deposits of the Lower Evenki Member (Middle Cambrian) have been refined. Four types of dolomites are identified: with stromatolitic texture, clotted-peloidal, replacement crystalline without preservation of primary protolith structures, and replacement variably-crystalline with a relict silt-pelitic structure of the protolith. Post-sedimentary alterations of the rocks are associated with multi-stage dolomitization processes – early, syngenetic, observed in types of dolomites with stromatolitic texture and/or bacterial structures, and later, identified in lithological types of replacement dolomites and silt-sandstones with dolomitic cement.

The elemental composition of carbonate (dolomites) and terrigenous (dolomitic siltstones and dolomitic argillites, sandstones and arkosic silt-sandstones with basal dolomitic cement) rocks has been studied. A heat map with clustering was used to visualize the general pattern of trace element distribution. Carbonate types are significantly enriched in Co, Cr, Sc, Rb and depleted in Cu, Zn, Li, Ba, Pb, and Sr in comparison with carbonate clarke values. The clastic part of the dolomites contains

quartz, Fsp (orthoclases, acid plagioclases), micas (biotite and muscovite), fragments of gneisses, quartzites, acid effusives, ferruginous siliceous rocks, and siderites.

The nature of the positive Eu anomaly, characteristic of both carbonate and terrigenous rocks, has been studied. Its origin is likely related to Eu-bearing minerals (plagioclases) in the terrigenous component, rather than to hydrothermal solutions. No direct correlation is observed between the REE content and the amount of terrigenous admixture or the normative Fsp content; therefore, the influence of reducing conditions or the composition of the dolomitizing solution on the REE distribution cannot be ruled out.

The probable source of the terrigenous clastic material was the Precambrian terranes of the Yenisei Ridge, formed by island-arc and crystalline/metamorphic complexes, as well as recycled sedimentary material.

The authors express their gratitude to Laboratory Assistant T.S.Sergeeva from the Instrumental Analytics Facility of the Paleontological Institute RAS and Assistant V.V.Pugach from the Department of Mineralogy and Petrography of Perm State National Research University for their assistance in performing the analytical work.

REFERENCES

1. Melnikov N.V. Vendian-Cambrian saline basin of the Siberian Platform. Stratigraphy, history of development. Novosibirsk: Sibirskii nauchno-issledovatelskii institut geologii, geofiziki i mineralnogo syrya, 2018, p. 177 (in Russian).
2. Regional stratigraphic scheme of the Cambrian deposits of the Siberian Platform. Explanatory note: Decisions of the All-Russian Stratigraphic Meeting on the development of regional stratigraphic schemes for the Upper Precambrian and Paleozoic of Siberia (Novosibirsk, 2012) (Cambrian of the Siberian Platform). Ed. by S.S.Sukhova, T.V.Pegel, Yu.Ya.Shabanova. Novosibirsk: Sibirskii nauchno-issledovatelskii institut geologii, geofiziki i mineralnogo syrya, 2021, p. 60 (in Russian).
3. Merenkova S.I., Puzik A.Yu., Afonin I.V. et al. The Formation Conditions of the Evenki Formation in the Lower Reaches of the Podkamennaya Tunguska River. *Moscow University Bulletin. Series 4. Geology.* 2024. N 1, p. 25-37 (in Russian). DOI: 10.55959/MSU0579-9406-4-2024-63-1-25-37
4. Saraev S.V., Khomenko A.V., Baturina T.P. et al. Vendian and Cambrian of the southeast of Western Siberia: stratigraphy, sedimentology, paleogeography. *Geologiya, geofizika i razrabotka neftyanykh i gazovykh mestorozhdenii*. 2004. N 1, p. 7-18 (in Russian).
5. Merenkova S.I. Cambrian paleobasin of the south of the Siberian Platform: geochemical and paleogeographical characteristics: Avtoref. dis. ... kand. geol.-mineral. nauk. Moscow: Moskovskii gosudarstvennyi universitet imeni M.V.Lomonosova, 2024, p. 21 (in Russian).
6. Kuznetsov V.G., Zhuravleva L.M. Pore Space in Carbonate Tidalites: Paleoclimatic Aspect. *Lithology and Mineral Resources.* 2019. Vol. 54. N 4, p. 320-332. DOI: 10.1134/S0024490219040047
7. Kuznetsov V.G., Ilyukhin L.N., Postnikova O.V. et al. Ancient carbonate sequences of Eastern Siberia and their oil and gas potential. Moscow: Nauchnyi mir, 2000, p. 104 (in Russian).
8. Plyusnin A.V. Structural model of the Vendian section belonging to the north-eastern part of the Nepa-Botuoba Anteclise, based on the structural cross-sections and sequence-stratigraphic modeling concerning Nepa Arch and Mirny Ridge areas. *Neftegazovaya geologiya. Teoriya i praktika.* 2019. Vol. 14. N 3, p. 39 (in Russian). DOI: 10.17353/2070-5379/30_2019
9. Plusnin A.V., Ivanova N.A., Sentyakova N.S. et al. Structure and formation conditions of the Yarakta productive horizon of the Late Vendian in the southern part of the Nepsko-Botuobinskaya Anticlise. *Bulletin of the Tomsk Polytechnic University. Geo Assets Engineering.* 2023. Vol. 334. N 11, p. 80-93 (in Russian). DOI: 10.18799/24131830/2023/11/4137
10. Qingqing Luo, Bo Liu, Kaibo Shi et al. The moldic pore evolution of the Middle Ordovician sabkha dolostone in Ordos Basin, China: A study based on the petrographic and geochemical characteristics of pore fillings. *Geological Journal*. 2022. Vol. 57. Iss. 7, p. 2812-2827. DOI: 10.1002/gj.4441
11. Guwei Xie, Fanwei Meng, Meifang Ye et al. Stromatolites from the Majiagou Formation in the Ordos Basin, Northwestern China. *Palaeogeography, Palaeoclimatology, Palaeoecology*. 2024. Vol. 633. N 111879. DOI: 10.1016/j.palaeo.2023.111879
12. Ying Xiong, Li-Chao Wang, Xiu-Cheng Tan et al. Dolomitization of the Ordovician subsalt Majiagou Formation in the central Ordos Basin, China: fluid origins and dolomites evolution. *Petroleum Science*. 2021. Vol. 18. Iss. 2, p. 362-379. DOI: 10.1007/s12182-020-00522-1
13. Misra S., Osogba O., Powers M. Chapter 1 — Unsupervised outlier detection techniques for well logs and geophysical data. Machine Learning for Subsurface Characterization. Gulf Professional Publishing, 2020, p. 1-37. DOI: 10.1016/B978-0-12-817736-5.00001-6
14. Rosen O.M., Abbyasov A.A. The Quantitative Mineral Composition of Sedimentary Rocks: Calculation from Chemical Analyses and Assessment of Adequacy (MINLITH Computer Program). *Lithology and Mineral Resources.* 2003. Vol. 38. N 3, p. 252-264. DOI: 10.1023/A:1023935803751

15. Rosen O.M., Abbyasov A.A., Migdisov A.A., Yaroshevskii A.A. MINLITH – A Program to Calculate the Normative Mineralogy of Sedimentary Rocks: the Reliability of Results Obtained for Deposits of Old Platforms. *Geochemistry International*. 2000. Vol. 38. N 4, p. 388-400.

16. Kuznetsov A.B., Semikhatov M.A., Gorokhov I.M. The Sr Isotope Chemostratigraphy as a Tool for Solving Stratigraphic Problems of the Upper Proterozoic (Riphean and Vendian). *Stratigraphy and Geological Correlation.* 2014. Vol. 22. N 6, p. 553-575. DOI: 10.1134/S0869593814060033

17. Kuznetsov A.B., Semikhatov M.A., Maslov A.V. et al. New Data on Sr- and C-Isotopic Chemostratigraphy of the Upper Riphean Type Section (Southern Urals). *Stratigraphy and Geological Correlation.* 2006. Vol. 14. N 6, p. 602-628. DOI: 10.1134/S0869593806060025

18. Pokrovskii B.G., Melezhik V.A., Bujakaite M.I. Carbon, Oxygen, Strontium, and Sulfur Isotopic Compositions in Late Precambrian Rocks of the Patom Complex, Central Siberia: Communication 1. Results, Isotope Stratigraphy, and Dating Problems. *Lithology and Mineral Resources.* 2006. Vol. 41. N 5, p. 450-474. DOI: 10.1134/S0024490206050063

19. Podkovyrov V.N., Semikhatov M.A., Kuznetsov A.B. et al. Carbonate Carbon Isotopic Composition in the Upper Riphean Stratotype, the Karatau Group, Southern Urals. *Stratigraphy and Geological Correlation.* 1998. Vol. 6. N 4, p. 319-335.

20. Montañez I.P., Osleger D.A., Banner J.L. et al. Evolution of the Sr and C Isotope Composition of Cambrian Oceans. *GSA Today*. 2000. Vol. 10. N 5, p. 1-7.

21. Saltzman M.R. Phosphorus, nitrogen, and the redox evolution of the Paleozoic oceans. *Geology*. 2005. Vol. 33. N 7, p. 573-576. DOI: 10.1130/G21535.1

22. Burns S.J., Mckenzie J.A., Vasconcelos C. Dolomite formation and biogeochemical cycles in the Phanerozoic. *Sedimentology*. 2000. Vol. 47. Suppl. 1, p. 49-61. DOI: 10.1046/j.1365-3091.2000.00004.x

23. Mazzullo S.J. Organogenic Dolomitization in Peritidal to Deep-Sea Sediments. *Journal of Sedimentary Research*. 2000. Vol. 70. N 1, p. 10-23. DOI: 10.1306/2DC408F9-0E47-11D7-8643000102C1865D

24. Vasconcelos C., McKenzie J., Bernasconi S. et al. Microbial mediation as a possible mechanism for natural dolomite formation at low temperatures. *Nature*. 1995. Vol. 377. Iss. 6546, p. 220-222. DOI: 10.1038/377220a0

25. Evdokimov A.N., Pharoe B.L. Features of the mineral and chemical composition of the Northwest manganese ore occurrence in the Highveld region, South Africa. *Journal of Mining Institute.* 2021. Vol. 248, p. 195-208. DOI: 10.31897/PMI.2021.2.4

26. Evdokimov A.N., Pharoe B.L. Indicator role of rare and rare-earth elements of the North-west manganese ore occurrence (South Africa) in the genetic model of supergene manganese deposits. *Journal of Mining Institute.* 2021. Vol. 252, p. 814-825. DOI: 10.31897/PMI.2021.6.4

27. Miura N., Kawabe I. Dolomitization of limestone with $MgCl_2$ solution at 150 °C: Preserved original signatures of rare earth elements and yttrium as marine limestone. *Geochemical Journal*. 2000. Vol. 34. Iss. 3, p. 223-227. DOI: 10.2343/geochemj.34.223

28. Elderfield H., Greaves M.J. The rare earth elements in seawater. *Nature*. 1982. Vol. 296. Iss. 5854, p. 214-219. DOI: 10.1038/296214a0

29. Kawabe I., Toriumi T., Ohta A., Miura N. Monoisotopic REE abundances in seawater and the origin of seawater tetrad effect. *Geochemical Journal*. 1998. Vol. 32. Iss. 4, p. 213-229. DOI: 10.2343/geochemj.32.213

30. Lichao Wang, Wenxuan Hu, Xiaolin Wang et al. Seawater normalized REE patterns of dolomites in Geshan and Panlongdong sections, China: Implications for tracing dolomitization and diagenetic fluids. *Marine and Petroleum Geology*. 2014. Vol. 56, p. 63-73. DOI: 10.1016/j.marpetgeo.2014.02.018

31. Ying Ren, Dakang Zhong, Chonglong Gao et al. The paleoenvironmental evolution of the Cambrian Longwangmiao Formation (Stage 4, Toyonian) on the Yangtze Platform, South China: Petrographic and geochemical constrains. *Marine and Petroleum Geology*. 2019. Vol. 100, p. 391-411. DOI: 10.1016/j.marpetgeo.2018.10.022

32. Nozaki Y. Elemental distribution. Overview. Encyclopedia of Ocean Sciences. Academic Press, 2001, p. 840-845. DOI: 10.1006/rwos.2001.0402

33. Taylor S.R., McLennan S.M. The Continental Crust: Its Composition and Evolution. Blackwell Scientific Publications, 1985, p. 312.

34. Bau M., Dulski P. Distribution of yttrium and rare-earth elements in the Penge and Kuruman iron-formations, Transvaal Supergroup, South Africa. *Precambrian Research*. 1996. Vol. 79. Iss. 1-2, p. 37-55. DOI: 10.1016/0301-9268(95)00087-9

35. Taylor S.R., McLennan S.M. The composition and evolution of the continental crust: rare earth element evidence from sedimentary rocks. *Philosophical Transactions of the Royal Society A*. 1981. Vol. 301. Iss. 1461, p. 381-399. DOI: 10.1098/rsta.1981.0119

36. Letnikova E.F. The REE distribution in carbonate rocks of different geodynamic types: Evidence from the southern folded framing of the Siberian platform. *Doklady Earth Sciences.* 2003. Vol. 393. N 8, p. 1180-1184.

37. Letnikova E.F., Kuznetsov A.B., Vishnevskaya I.A. et al. The Vendian passive continental margin in the southern Siberian Craton: geochemical and isotopic (Sr, Sm-Nd) evidence and U-Pb dating of detrital zircons by the LA-ICP-MS method. *Russian Geology and Geophysics.* 2013. Vol. 54. N 10, p. 1177-1194. DOI: 10.1016/j.rgg.2013.09.004

38. Shannon R.D. Revised effective ionic radii and systematic studies of interatomic distances in halides and chalcogenides. *Acta Crystallographica Section A*. 1976. Vol. 32. Iss. 5, p. 751-767. DOI: 10.1107/S0567739476001551

39. Lakshtanov L.Z., Stipp S.L.S. Experimental study of europium (III) coprecipitation with calcite. *Geochimica et Cosmochimica Acta*. 2004. Vol. 68. Iss. 4, p. 819-827. DOI: 10.1016/j.gca.2003.07.010

40. Kučera J., Cempírek J., Dolníček Z. et al. Rare earth elements and yttrium geochemistry of dolomite from post-Variscan vein-type mineralization of the Nízký Jeseník and Upper Silesian Basins, Czech Republic. *Journal of Geochemical Exploration*. 2009. Vol. 103. Iss. 2-3, p. 69-79. DOI: 10.1016/j.gexplo.2009.08.001

41. Schwinn G., Markl G. REE systematics in hydrothermal fluorite. *Chemical Geology*. 2005. Vol. 216. Iss. 3-4, p. 225-248. DOI: 10.1016/j.chemgeo.2004.11.012

42. Bau M. Rare-earth element mobility during hydrothermal and metamorphic fluid-rock interaction and the significance of the oxidation state of europium. *Chemical Geology*. 1991. Vol. 93. Iss. 3-4, p. 219-230. DOI: 10.1016/0009-2541(91)90115-8

43. Banner J.L. Application of the trace element and isotope geochemistry of strontium to studies of carbonate diagenesis. *Sedimentology*. 1995. Vol. 42. Iss. 5, p. 805-824. DOI: 10.1111/j.1365-3091.1995.tb00410.x

44. Vasileva K.Yu. Stages of post-sedimentary alterations of the Riphean–Vendian carbonate rocks of the Kuyumba deposit and its connection with the geological evolution of the Baykit Anteclise (southwest of the Siberian Platform): Avtoref. dis. ... kand. geol.-mineral. nauk. Saint Petersburg: Sankt-Peterburgskii gosudarstvennyi universitet, 2017, p. 21 (in Russian).

45. Grigoriev N.A. Chemical element distribution in the upper continental crust. Ekaterinburg: Institute of Geology and Geochemistry, Urals Branch of RAS, 2009, p. 381 (in Russian).

46. Floyd P.A., Leveridge B.E. Tectonic environment of the Devonian Gramscatho basin, south Cornwall: framework mode and geochemical evidence from turbiditic sandstones. *Journal of the Geological Society*. 1987. Vol. 144. N 4, p. 531-542. DOI: 10.1144/gsjgs.144.4.0531

47. Cullers R.L. Implications of elemental concentrations for provenance, redox conditions, and metamorphic studies of shales and limestones near Pueblo, CO, USA. *Chemical Geology*. 2002. Vol. 191. Iss. 4, p. 305-327. DOI: 10.1016/S0009-2541(02)00133-X

48. Vernikovsky V.A., Vernikovskaya A.E. Tectonics and evolution of granitoid magmatism in the Yenisei Ridge. *Russian Geology and Geophysics.* 2006. Vol. 47. N 1, p. 35-52.

49. Vernikovsky V.A., Vernikovskaya A.E., Nozhkin A.D., Ponomarchuk V.A. Riphean ophiolites of the Isakov belt (Yenisei Ridge). *Geologiya i geofizika*. 1994. Vol. 35. N 7-8, p. 169-181 (in Russian).

50. Priyatkina N.S., Kuznetsov N.B., Shatsillo A.V. et al. U/Pb dating of zircons from Late Precambrian and Early Paleozoic sandstones of the Yenisei Ridge. Geodinamicheskaya evolyutsiya litosfery Tsentralno-Aziatskogo podvizhnogo poyasa (ot okeana k kontinentu): Materialy nauchnogo soveshchaniya, 11-14 oktyabrya 2016, Irkutsk, Rossiya. Irkutsk: Institut zemnoi kory SO RAN, 2016. Iss. 14, p. 230-232 (in Russian).

51. Kuznetsov N.B., Shatsillo A.V., Romanyuk T.V. et al. Primary sources of zircon in clastic rocks of the Neoproterozoic and Lower Paleozoic sequences of the East Angara zone (north of the Yenisei Ridge). Fundamentalnye problemy izucheniya vulkanogenno-osadochnykh, terrigennykh i karbonatnykh kompleksov: Materialy Vserossiiskogo litologicheskogo soveshchaniya, posvyashchennogo pamyati A.G.Kossovskoi i I.V.Khvorovoi, 11-12 noyabrya 2020, Moskva, Rossiya. Moscow: GEOS, 2020, p. 118-123 (in Russian).

***Authors*: Sofya I. Merenkova,** *Candidate of Geological and Mineralogical Sciences, Researcher* (*Shirshov Institute of Oceanology of RAS, Moscow, Russia*), *Junior Researcher* (*Schmidt Institute of Physics of the Earth RAS, Moscow, Russia*), *koshelevasof@mail.ru*, *https://orcid.org/0000-0003-3204-4393*, **Evgeniya V. Karpova,** *Candidate of Geological and Mineralogical Sciences, Associate Professor* (*Lomonosov Moscow State University, Moscow, Russia*), *https://orcid.org/0000-0003-3094-2253*, **Aleksei Yu. Puzik,** *Senior Lecturer* (*Perm State National Research University, Perm, Russia*), *https://orcid.org/0000-0001-7148-7344*, **Vladimir A. Litvinskii,** *Candidate of Biological Sciences, Senior Researcher* (*Borissiak Paleontological Institute of RAS, Moscow, Russia*), *https://orcid.org/0000-0003-2045-4002*, **Yuliya V. Shuvalova,** *PhD, Researcher* (*Borissiak Paleontological Institute of RAS, Moscow, Russia*), *https://orcid.org/0000-0002-5075-6952*, **Margarita A. Volkova,** *Candidate of Chemical Sciences, Associate Professor* (*Perm State National Research University, Perm, Russia*), *https://orcid.org/0000-0002-3416-8296*, **Aleksei A. Medvedkov,** *Candidate of Geography, Associate Professor* (*Lomonosov Moscow State University, Moscow, Russia*), *Senior Researcher* (*Institute of Geography RAS, Moscow, Russia*), *https://orcid.org/0000-0002-7242-7172*.

The authors declare no conflict of interests.